46th AIAA Aerospace Sciences Meeting and Exhibit
7 - 10 January 2008, Reno, Nevada

AIAA 2008-508

DNS of Reacting H_2/Air Laminar Vortex Rings

Jeff Doom* and Krishnan Mahesh†

University of Minnesota, Minneapolis, MN, 55455, USA

Direct numerical simulation (DNS) is used to study reacting, laminar vortex rings. A novel, all–Mach number algorithm developed by Doom, Hou, & Mahesh[1] is used. The chemical mechanism is a nine species, nineteen reaction mechanism for H_2/Air from Mueller at el.[2] Diluted H_2 at ambient temperature (300 K) is injected into hot air (1200 K & 1800 K). The simulations study the effect of Damkohler number, initial oxidizer temperature and stroke length.

I. Introduction

The motion of a fluid column of length L through an orifice of diameter D produces a vortex ring. Non–reacting vortex rings have been studied by many researchers, and a large volume of work exists (e.g. the review by Shariff and Leonard[3]). Less is known about reacting vortex rings. This paper is motivated by the relevance of vortex rings to the fuel injection problem, where a piston pushes a ring of gaseous fuel into hot oxidizer.

Our objective is to predict and understand the injection process, particularly as it applies to H_2/air. Related experiments and simulations are those by Chen et al.[4,5,6] where they studied propane/air and ethane/air. Chen et al.'s simulations use a conserved scalar approach where the chemical species and temperature are functions of the conserved scalar and scalar dissipation rate. Also, Hewett and Madnia[7] use a one–step chemical mechanism to study methane/air reacting vortex rings.

This paper considers the situation where a round nozzle injects fuel ($H_2 + N_2$) at room temperature into oxidizer ($O_2 + N_2$) at high temperatures. The amount of fuel injected, is controlled by the stroke length. The three–dimensional, unsteady, compressible, Navier-Stokes equations are used, along with conservation equations for the nine species described by the Mueller et al.[2] chemical mechanism. Our objective is to study the effects of Damkohler number, stroke length, and oxidizer temperature.

II. Simulation Details

II.A. Governing Equations

The governing equations are the unsteady, compressible, reacting Navier–Stokes equations. From Doom et al.,[1] they are in non–dimensional form:

$$\frac{\partial \rho}{\partial t} + \frac{\partial \rho u_j}{\partial x_j} = 0, \tag{1}$$

$$\frac{\partial \rho Y_k}{\partial t} + \frac{\partial \rho Y_k u_j}{\partial x_j} = \frac{1}{ReSc_k}\frac{\partial}{\partial x_j}\left(\mu \frac{\partial Y_k}{\partial x_j}\right) + \dot{\omega}_k, \tag{2}$$

$$\frac{\partial \rho u_i}{\partial t} + \frac{\partial \rho u_i u_j}{\partial x_j} = -\frac{\partial p}{\partial x_i} + \frac{1}{Re}\frac{\partial \tau_{ij}}{\partial x_j}, \tag{3}$$

*Graduate Research Assistant
†Associate Professor

$$M_r^2\left[\frac{\partial}{\partial t}\left(p+\frac{\gamma-1}{2}\rho u_i u_i\right)+\frac{\partial}{\partial x_j}\left(\gamma p+\frac{\gamma-1}{2}\rho u_i u_i\right)u_j\right]+\frac{\partial u_j}{\partial x_j}$$
$$=\frac{(\gamma-1)M_r^2}{Re}\frac{\partial \tau_{ij}u_i}{\partial x_j}+\frac{1}{RePr}\frac{\partial}{\partial x_j}\left(\frac{\mu}{W}\frac{\partial T}{\partial x_j}\right)+\underbrace{\sum_{k=1}^{N}Q_k\dot{\omega}_k}_{\dot{\omega}_n}. \tag{4}$$

$$\frac{\rho T}{W}=\gamma M_r^2 p+1. \tag{5}$$

Here, ρ, T, p, u_i and Y_k denote non–dimensional density, temperature, pressure, velocities and mass fraction of 'k' species respectively. The viscous stress tensor is defined as: $\tau_{ij}=\mu\left(\frac{\partial u_i}{\partial x_j}+\frac{\partial u_j}{\partial x_i}-\frac{2}{3}\frac{\partial u_k}{\partial x_k}\delta_{ij}\right)$. The source term is denoted as: $\dot{\omega}_k$ which is modeled using the Arrhenius law. The heat of reaction per unit mass in the energy equation is Q_k and $\sum Q_k\dot{\omega}_k$ or $\dot{\omega}_n$ is the heat release due chemical reactions. Sc_k is the Schmidt number for the k^{th} species, Pr is the Prandtl number, and Re is the Reynolds number. W is the mean molecular weight of the mixture.

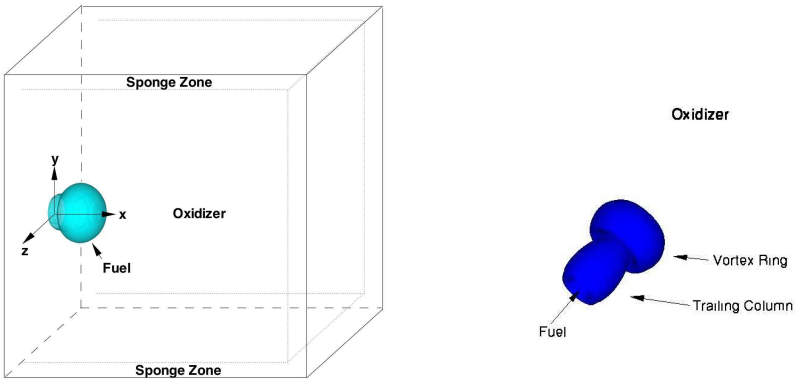

(a) (b)

Figure 1. A schematic of the problem and vocabulary of the problem

II.B. Numerical Method

Note that (Doom et al.[1]) the Navier–Stokes equations are non–dimensionalized using an incompressible scaling for pressure i.e. $p=\frac{p^d-p_r}{\rho_r u_r^2}$. The energy equation is then interpreted as an equation for the divergence of velocity. As a result, when the reference Mach number is zero (M_r), the non-dimensional reacting governing equations reduce to:

$$\frac{\partial \rho}{\partial t}+\frac{\partial \rho u_j}{\partial x_j}=0, \tag{6}$$
$$\frac{\partial \rho u_i}{\partial t}+\frac{\partial \rho u_i u_j}{\partial x_j}=-\frac{\partial p}{\partial x_i}+\frac{1}{Re}\frac{\partial \tau_{ij}}{\partial x_j}, \tag{7}$$
$$\frac{\partial \rho Y_k}{\partial t}+\frac{\partial \rho Y_k u_j}{\partial x_j}=\frac{1}{ReSc_k}\frac{\partial}{\partial x_j}\left(\mu\frac{\partial Y_k}{\partial x_j}\right)+\dot{\omega}_k, \tag{8}$$

$$\frac{\partial u_j}{\partial x_j} = \frac{1}{RePr}\frac{\partial}{\partial x_j}\left(\frac{\mu}{W}\frac{\partial T}{\partial x_j}\right) + \sum_{k=1}^{N} Q_k \dot{\omega}_k, \tag{9}$$

$$\frac{\rho T}{W} = 1. \tag{10}$$

Notice that the divergence of velocity equals the sum of the terms involving thermal conduction and heat release. If the density is constant and there is no heat release, the energy equation reduces to the incompressible continuity equation. In the presence of heat release, the zero Mach number reacting equations (Majda & Sethian[8]) are obtained.

The numerical algorithm is discussed in detail by Doom et al.[1] The algorithm is fully implicit, spatially non–dissipative and second order in time & space. The thermodynamic variables and species are staggered in time from velocity. All variables are co–located in space. A pressure–correction method is used. The discrete equations discretely conserve kinetic energy in the incompressible, non–reacting, inviscid limit. These features make the algorithm stable and accurate at high Reynolds numbers.

II.C. Problem statement

Table 1. Inlet boundary conditions and Control stroke length

Inlet variables	
T_{in}	$(T_O - T_F)\left(1 - \left[\frac{1}{2} - \frac{1}{2}\tanh\left(10\left[\sqrt{y^2+z^2} - 1\right]\right)\right]\right) + T_F$
u_{in}	$u_F\left(\frac{1}{2} - \frac{1}{2}\tanh\left[10\left(\sqrt{y^2+z^2} - 1\right)\right]\right) U_{time}$
$Y_{H_2,in}$	$Y_{F_0}\left(\frac{1}{2} - \frac{1}{2}\tanh\left[10\left(\sqrt{y^2+z^2} - 1\right)\right]\right) U_{time}$
$Y_{O_2,in}$	$Y_{O_0}\left(1 - \left[\frac{1}{2} - \frac{1}{2}\tanh\left(10\left[\sqrt{y^2+z^2} - 1\right]\right)\right]\right)$
p_{in}	0
rho_{in}	$\frac{MW_{in}}{T_{in}}$

Figure 1 (a) shows a schematic of the problem and figure 1 (b) illustrates the ring vortex and the trailing column. The dimensional variables for the reacting vortex ring are chosen such that the equivalence ratio, ϕ, is one, and a stoichiometric mixture is obtained where $Y_{H_2,0}$ equals 0.029 and $Y_{O_2,0}$ equals 0.232. For the simulations, Re is 1000 and Pr is 0.7. μ is equal to $T^{0.7}$ and Sc_k is set to 0.70 such that $Le_k = 1$.

The inflow boundary conditions are shown in table (1). Note that T_O is the temperature of the oxidizer and T_F is the temperature of the fuel. u_F is the fuel velocity coming out of the nozzle. Y_{F_0} is the mass fuel fraction and Y_{O_0} is the mass oxidizer fraction. U_{time} controls the duration of stroke length (L/D). Note that all reference variables are non-dimesionalized with respect to the fuel side.

The boundary conditions are as follows. The inflow is set to a constant value for thermodynamic variables, species, and the velocities which is shown in table 1. The first derivative is set to zero for thermodynamic variables, species, and velocities at the outflow. At the y and z boundaries, the thermodynamic variables and species are set to a constant (same as initial conditions) and the velocities are set to zero. 'Sponge' boundary conditions (Colonius et al.[9]) are used at the outflow, and transverse boundaries to absorb acoustic waves that are generated by the initial transient. A cooling term, $-\sigma\left(U - U_{ref}\right)$ is added to the right hand side of the governing equations over the sponge zone whose length is 10 percent of the domain. Here U and U_{ref} denote the vector of conservative variables and the 'reference' solution respectively. The coefficient σ for the sponge at the outflow, is a polynomial function defined as:

$$\sigma\left(x\right) = A_s \frac{\left(x - x_s\right)^n}{\left(L_x - x_s\right)^n}, \tag{11}$$

where x_s and L_x denotes the start of the sponge and the length of the domain. n and A_s are equal to three.

III. Results

III.A. Validation

The simulations are validated using a one–step chemical mechanism, and compared to the one-step simulations of Hewett & Madnia.[7] The temperature ratio T_{amb}/T_{jet} allows ignition to happen either in the formation or post-formation of the reacting vortex ring. If the ambient temperature is relatively low, there will be a ignition delay after the formation of the vortex ring. For higher temperatures, ignition occurs rapidly and most of the reaction is in front of the vortex, which is shown in figure 2 (a). Our results are compared to case 5 in their paper where the temperature ratio is 6:1 and the stroke length is two which is presented in figure 2 (b). Note that good agreement is obtained.

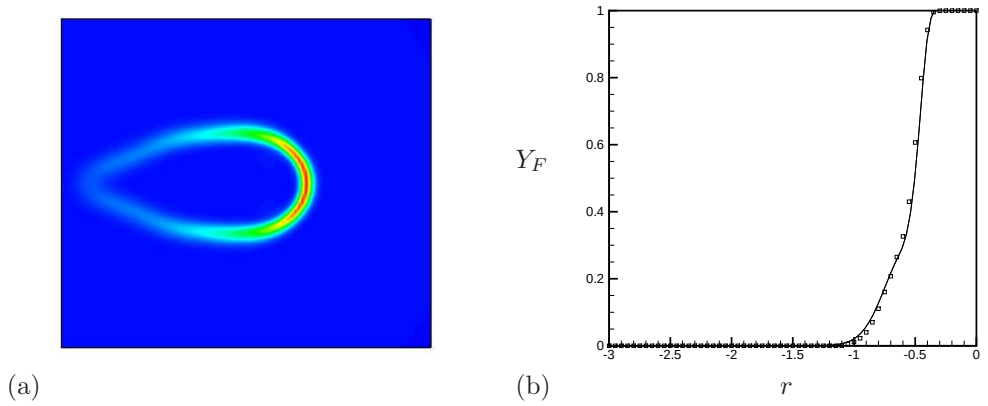

Figure 2. (a) heat release, $\dot{\omega}_k$, and (b) comparison to Hewett and Madnia. – Present and □ Hewett & Madnia.

III.B. Reacting H_2/Air Vortex Ring

Table 2. Parameters of H_2 – Air reacting vortex ring.

$T_O(K)$	$\tau_r(sec)$	Stroke Length ($\frac{L}{D}$)	inlet velocity (m/s)	(Da)
1200	$7.0e{-}5$	2.0	141	2.3
1200	$7.0e{-}4$	2.0	14.1	23
1200	$7.0e{-}5$	6.0	141	2.3
1800	$7.0e{-}5$	2.0	141	2.3

The cases that will be studied are listed in table 2. The first parameter that will be studied is the effect of Damkohler number, Da, where Da is defined as: $Da = \frac{\tau_r}{\tau_{chem}}$. τ_{chem} is the chemical time scale which is determined by the chemical mechanism where τ_{chem} is approximately $3.0e-5$ (sec). τ_r is the flow time scale. The next parameter that will be studied is the stroke length of the reacting vortex ring. The simulation studies two different stroke lengths of 2 and 6. The choice in these two stroke lengths was motivated by Sau & Mahesh[10] who studied scalar mixing in non–reacting vortex rings. Another parameter that will be studied is the initial temperature of the oxidizer. Oxidizer temperature of 1200 and 1800 Kelvin will be considered.

III.B.1. Effect of Stroke length at low Damkohler Number

We consider a stroke length of two at low Damkohler number. H_2 at a temperature of 300 K is injected into air at 1200 K. As the fuel convects through the domain, the fuel and oxidizer diffuse together, forming products. Once non–dimensional time reaches 2, the trailing column collapses and oxidizer is entrained behind the ring vortex. Since the Damkohler is low, there is an ignition delay which is illustrated in figure 3. Note that ignition occurs behind the core, and then propagates to the core where fuel is rapidly consumed. Due to entrainment, ideal mixing with fuel and oxidizer occurs behind the vortex ring. Since there is an ignition delay, this allows mixing to occur. Higher oxidizer temperature and high Da cause the fuel to ignite nearly instantaneously affecting the mixing of fuel and oxidizer. The reason behind this will be discussed in section III.B.3.

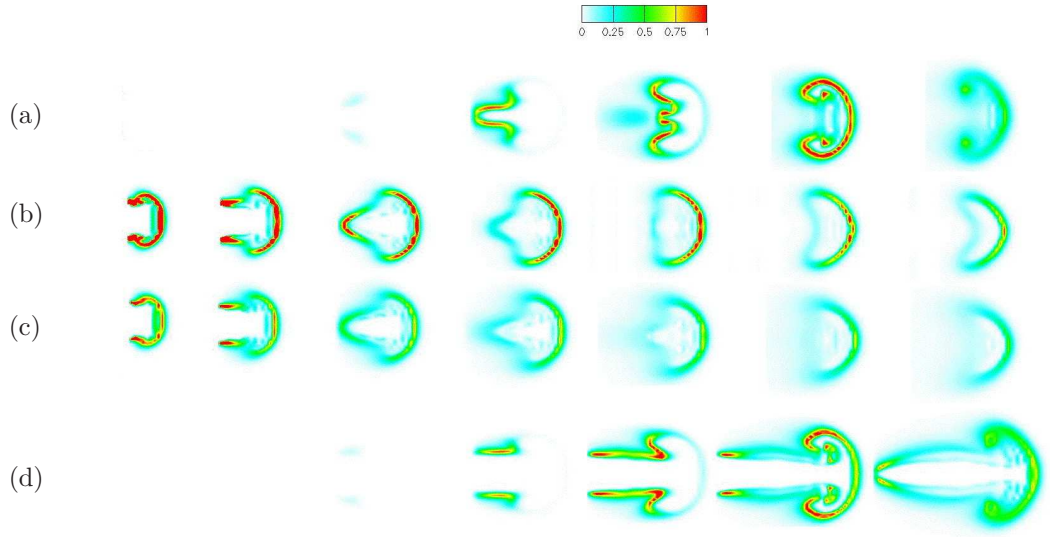

Figure 3. Time evolution (seven units of time) of heat release ($\dot{\omega}_n$). Each contour plot is one unit of time for a total of seven units of time. (a) Low Da at L/D of 2, (b) high Da at L/D of 2, (c) High Oxidizer Temperature at L/D of 2 and (d) low Da at L/D of 6

Once there is significant accumulation of HO_2 radicals ($Y_{HO_2} \sim 10^{-4}$), and temperature is close to activation temperature then ignition will occur. Once ignition occurs then the formation of H_2O will be seen. The reasoning behind this process is the activation energies in the formation and consumption of HO_2 is low in the Mueller mechanism (Reaction 9-13). Therefore, once the formation of HO_2 is adequate and also temperature is adequate, ignition will begin which is one of the four reactions in the H_2/O_2 chain reactions in the Mueller mechanism (Reaction 1-4). Once the chain-branching starts, rapid formation of OH and H_2O will occur. For the minor species, H,O, and H_2O_2, form along the interface of H_2 and air. Then the minor species will form major species H_2O and OH where the majority is water. Figure 5 illustrates the time evolution of species HO_2, H_2O_2, OH, and H_2O, respectively. Once the formation of water occurs, temperature will rise because the formation of enthalpy for water adds heat. Once the fuel is consumed (no heat release), the flame will reach a maximum temperature (burnout) where it is around 2163 K in the vortex core.

A comparison of the results from the reacting vortex ring to nonreacting vortex rings shows that the reacting vortex ring decelerates faster than the nonreacting vortex ring. This can be attributed to the decrease in the value of the core vorticity, which is caused by the heat of reaction (Hewett & Madnia[7]). A combination of expansion of the flow from heat release and the increase in viscosity from an increase in temperature decrease the core vorticity (figure 6 (a) and (b)). In the high Da case and higher temperature case, the decrease in vorticity is quite significant (figure 4 (b) and (c)). In the Low Da case, the vorticity

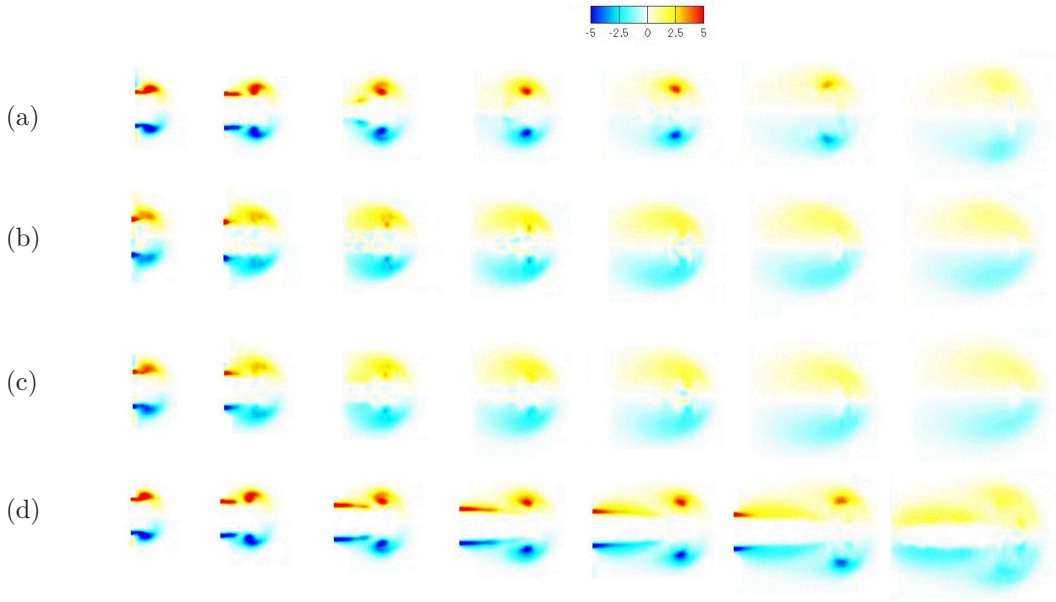

Figure 4. Time evolution of heat release (ω_z). Each contour plot is one unit of time for a total of seven units of time. (a) Low Da at L/D of 2, (b) high Da at L/D of 2, (c) High Oxidizer Temperature at L/D of 2 and (d) low Da at L/D of 6

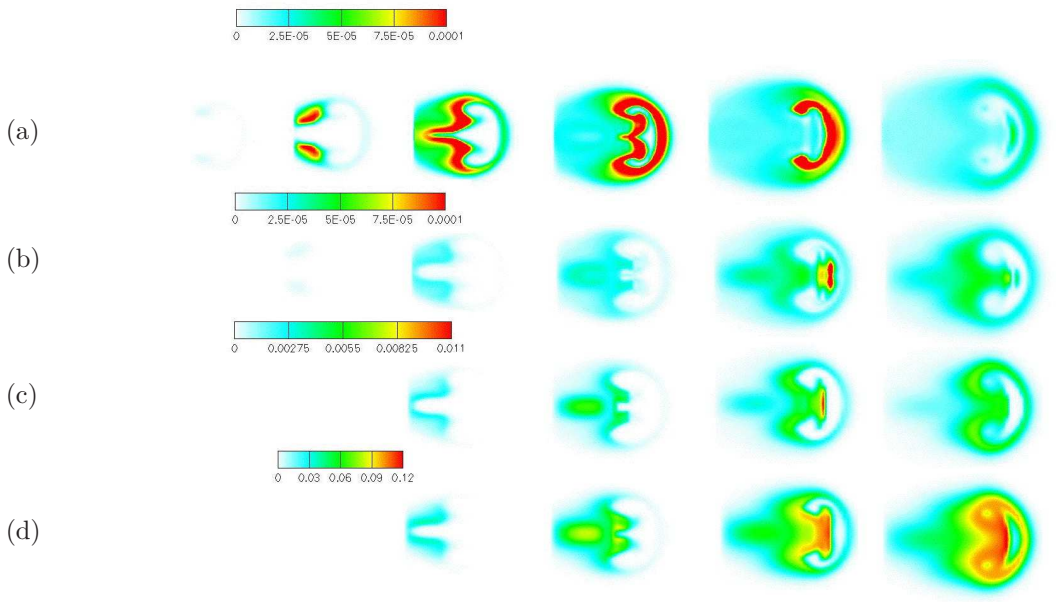

Figure 5. Time evolution of low Da at L/D of 2. Each contour plot is one unit of time for a total of seven units of time. (a) Y_{HO_2}, (b) $Y_{H_2O_2}$, (c) Y_{OH} and (d) Y_{H_2O}

behaves similar to the non–reacting case until ignition occurs (significant heat release). Our observations are consistent with Hewett & Madnia[7] and Chen & Dahm.[6] Both claim that dilatation is responsible for the increase in ring speed in the early stage and the sharp reduction in ring speed in the later stage due to heat release from chemical reactions. Figure 6 (c) and (d) shows a comparison between dilatation and the heat release term.

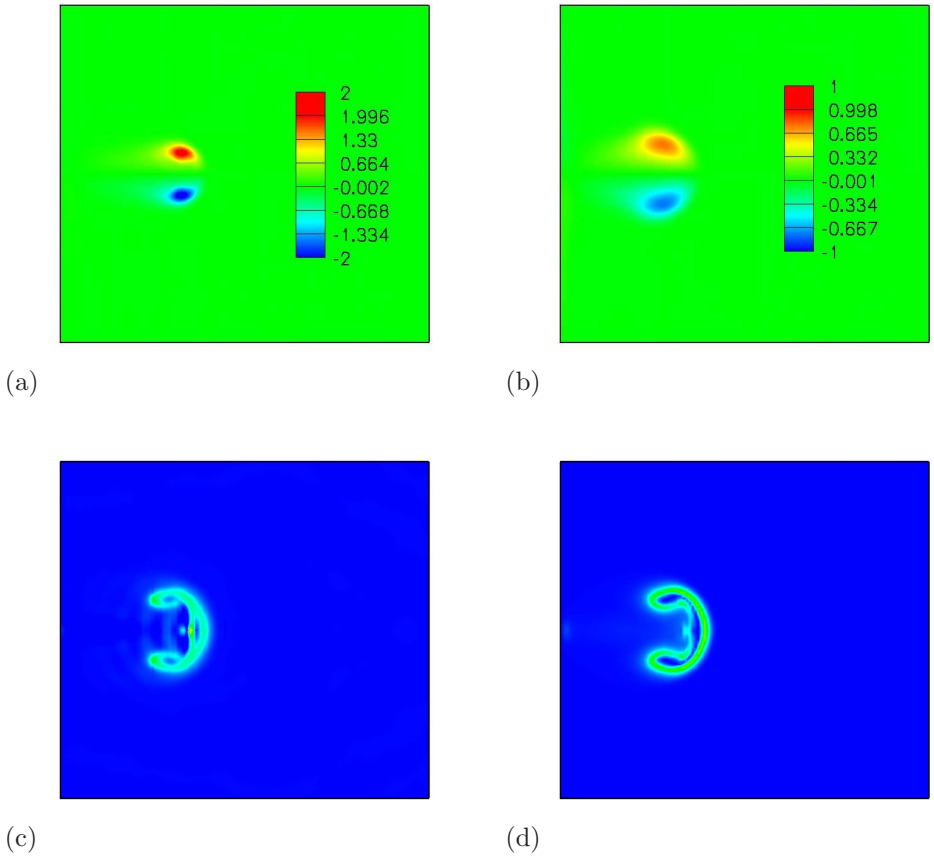

Figure 6. Contour plots of z-vorticity at L/D of 2 (a) non-reacting vortex ring and (b) reacting vortex ring at low Da. (c) is contour plot of divergence and (d) is a contour plot of heat release at L/D of 2 & low Da.

The reacting vortex of stroke length of 6 is initially similar to the reacting vortex ring of stroke length of 2 at low Damkohler. Since the trailing column does not close until L/D of 6, the difference will be clear after non–dimensional time of 2. An important observation is that ignition stills occurs about the same time as the stroke length of 2. The difference between the two different cases is that for stroke length of 2, ignition occurs behind the vortex. For stroke length of 6, ignition occurs along the trailing column instead of behind the vortex ring. This is shown in figure 3. There is a large rise in temperature along the trailing column. Instead of fluid entraining into the jet, one notices de-entrainment. Note in figures 4 (d) and 7 (a) that the trailing column is 'thicker' (compared to non–reacting vortex rings) which is caused by the de-entrainment. Also, note that the shape of the flame is conical and not a ring. The reason for the difference in shape is due to the extra fuel being injected. The inner part of the core is still cool, but the outer part of the core is expanding due to heat release. Therefore, the inner core will remain at the same speed but the outer core with slow down forming a conical shape.

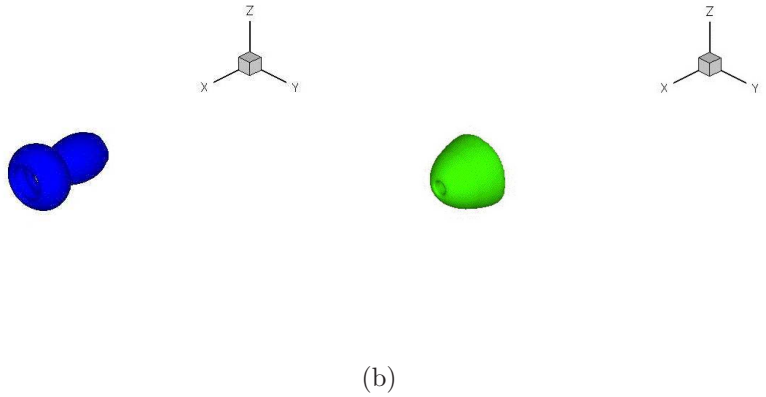

(a) (b)

Figure 7. Isosurface plot of z vorticity for stroke length of 6 where (a) is at a non–dimensional time of 5 and (b) is 10.

III.B.2. Effect of High Damkohler Number

At higher Damkohler number, ignition is nearly instantaneous. Instead of products forming behind the vortex ring, products form around the entire interface between H_2 and air. Therefore, this consumes the fuel more rapidly which initially expands the combustion area because the heat release term ($\dot{\omega}_n$) is around 30 times greater then the heat release term in the low Da case when ignition occurs. Since the heat release is higher, this causes the vorticity to drop immediately (figure 4 (b)). Figure 3 (b) illustrates the evolution of heat release at high Damkohler number. From Warnatz et al.,[11] the adiabatic flame temperature in a stoichiometric mixture is $2380K$ for H_2/air. The maximum temperature is around 2387 K in the vortex core and burnout time is smaller than the low Da case by a non-dimensional time of around 2. The max temperature is around a non–dimensional time of 9; afterward there is no more heat release. Thus, the temperature starts to drop i.e. the higher temperature will diffuse into the oxidizer temperature to cool the flame.

The effects of the global Damkohler number may also be observed by plotting the mixture fraction versus fuel or oxidizer. The mixture fraction is defined as (Hilbert & Thevenin[12]):

$$\zeta = \frac{\frac{1}{2}\frac{Y_F}{W_F} + \frac{Y_O^0 - Y_O}{W_O}}{\frac{1}{2}\frac{Y_F^0}{W_F} + \frac{Y_O^0}{W_O}}. \tag{12}$$

Figures 8 (a), (b), (c) and (d) correspond to low Da at L/D of 2, high Da at L/D of 2, low Da at L/D of 6 and high oxidizer temperature at L/D of 2, respectively. Note that □, □, and □ are non–dimensional times of 2,6, and 10, respectively. Figure 8 (a) shows the ignition delay compared to the faster chemistry in figure 8 (b) where the low Damkohler case does not reach the fast chemistry limit until burnout. Figure 8 (b) approaches the infinite fast chemistry limit more closely than figure 8 (a), (c) and (d) because of a higher Damkohler number. Note that in figure 8 (c) the stroke length of 6 reaches the fast chemistry limit because more fuel is being injected compared to the low Da case where burnout occurs much later in time. Figure 8 (d) is the higher oxidizer temperature. Notice that ignition is also nearly instantaneous compared to the high Da case.

III.B.3. Oxidizer Temperature of 1800 K

The higher oxidizer temperature yields similar results to the high Damkohler number case. Ignition is nearly instantaneous. Figure 3 (c) illustrates the time evolution of the heat release. At first glance, figures 3

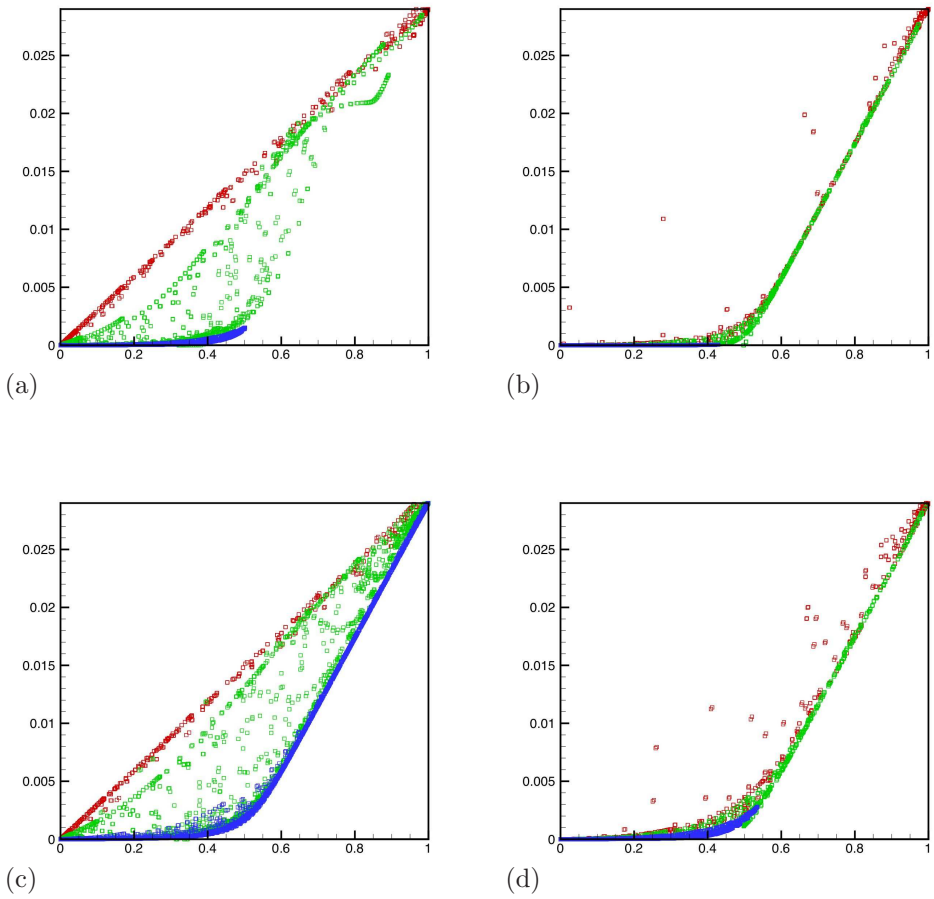

Figure 8. Scatter plot of ζ versus H_2. (a) low Damkohler number at $L/D = 2$, (b) high Damkohler number at $L/D = 2$, (c) low Damkohler number with a L/D of 6 and (d) initial oxidizer temperature of 1800 K at $L/D = 2$. □, □, and □ are a nondimensional time of 2,6, and 10, respectively.

(b) and 3 (c) look similar. The difference is that the high Damkohler case consumes fuel faster than the higher oxidizer temperature case which implies that the burnout time is faster as well. Burnout occurs at a non-dimensional time of 12 whereas the burnout time for the high Damkohler case is 9. For our study, the high Damkohler number had the fastest fuel burnout time at a nondimensional time of 9. Next was the low Damkohler number case at a nondimensional time of 11 and finally the higher oxidizer temperature of nondimensional time of 12. Changing the Damkohler number will change the amount of fuel being consumed. Increasing this factor will increase amount of fuel that is being consumed. Increasing the temperature will not increase the rate that fuel is being consumed. It will only increase the likelihood that a reaction in a given mechanism will occur. With higher temperatures, the reaction can occur because the temperature is high enough to overcome the activation energy require for the given reaction to occur. Hewett & Madnia found similar results comparing results of a low and high initial oxidizer temperature. They found that the total amount of formation in the lower oxidizer temperature produced more product later in time compared to the higher oxidizer temperature.

Figure 9 computes the average fuel mass fraction and the heat release versus time. Figure 9 (a) shows the fuel injection and consumption of fuel in time at stroke length of two. This figure clearly shows that at higher oxidizer temperature ignition is nearly instantaneous compared to the lower oxidizer temperature and fuel is being consumed at a faster rate at the beginning of the simulation. Note in figure 9 (b) that ignition is larger but there is also an ignition delay. In the high oxidizer temperature, ignition is nearly instantaneous which causes the flow to expand and dilation to increase. This decreases the vorticity at a faster rate compared to the low oxidizer temperature. Therefore, in the low oxidizer temperature there will be increased mixing due to the higher vorticity providing ideal conditions for rapid ignition. Since the flow expands, it effects the entrainment of the flow which is shown in figure 10. Note that in figure 10 (a) the velocity vectors entrain oxidizer directly into fuel behind the vortex whereas the velocity vectors turns towards the higher temperatures in figure 10 (b). Instead of pushing fresh oxidizer behind the core, the higher temperature pushes the fresh oxidizer into the higher temperature region where there is less fuel which chokes the flame. As a result, higher oxidizer temperatures consume fuel at a slower rate.

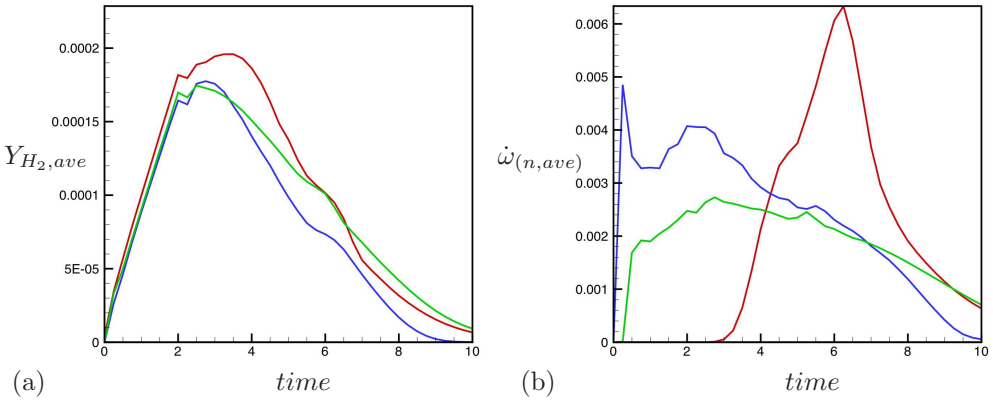

Figure 9. Domain average for low oxidizer temperature – , high oxidizer temperature – and high Damkohler – at L/D of 2.

IV. Acknowledgments

This work was supported by the AFOSR under grant FA9550–04–1–0341. Computing resources were provided by the Minnesota Super-computing Institute, the San Diego Super-computing Center and the

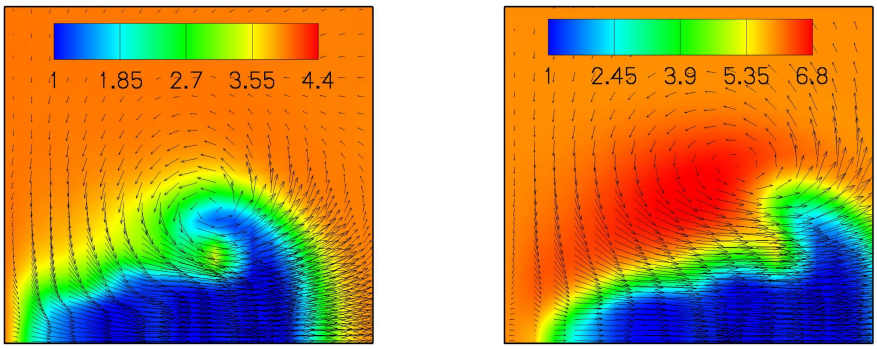

(a) (b)

Figure 10. Contour plot of T and velocities vectors at a nondimensional time of 2.5 at L/D of 2 (a) initial oxidizer temperature of 1200 K and (b) initial oxidizer temperature of 1800 K.

National Center for Super-computing Applications.

References

[1]J. Doom, Y. Hou, K. Mahesh, A numerical method for DNS/LES of turbulent reacting flows. *J. Comput. Phys.* **226** (2007) 1136–1151.

[2]M.A. Mueller, T.J. Kim, R.A. Yetter, F.L. Dryer, Flow Reactor Studies and Kinetic Modeling of the H2/O2 Reaction. *Int. J. Chem. Kinet.* **31** (1999) 113–125.

[3]K. Shariff, A. Leonard, Vortex rings. *Annu. Rev. Fluid. Mech.* **24** (1992) 235–279.

[4]S.L Chen, J.A. Dahm, Coupling Between Fluid Dynamics and Combustion in a Laminar Vortex Ring. *AIAA paper 2000–0433.* (2000).

[5]S.L Chen, J.A. Dahm, Results from Numerical Simulations of the Diffusion Flame-Vortex Ring Interaction. *AIAA paper 2000–2468.* (2000).

[6]S. Chen, W. Dahm, Effects of heat release in a reacting vortex ring. *Proc. Combust. Inst.*. **28** (2000).

[7]J.S. Hewett, C.K. Madnia, Flame–vortex interaction in a reacting vortex ring. *Phys. Fluids.* **10** (1998) 189–205.

[8]A. Majda, J.A. Sethian, The derivation and numerical solution of the equations for zero Mach number combustion. *Combust. Sci. Technol.* **42** (1985) 185–205.

[9]T. Colonius, P. Moin, & S.K. Lele, Direct Computation of Aerodynamic Sound. Report No. TF-65, Department of Mechanical Engineering, Stanford University, Stanford, California.

[10]R. Sau, K. Mahesh, Passive scalar mixing in vortex rings. *J. Fluid Mech.* **582** (2007) 449–461.

[11]J. Warnatz, U. Maas, & R.W. Dibble, Combustion: Physical and Chemical Fundamentals. *Springer*, 2001.

[12]R. Hilbert, D. Thevenin, Influence of differential diffusion on maximum flame temperature in turbulent nonpremixed hydrogen/air flames. *Combust. Flame.* **138** (2004) 175–187